Wash-free highly sensitive detection of C-reactive protein using gold derivatised triangular silver nanoplates

Yi Zhang,[a] Denise E. Charles,[b] Deirdre M. Ledwith,[c] Damian Aherne,[c] Stephen Cunningham,[a] Muriel Voisin,[a] Werner J. Blau,[b] Yurii K. Gun'ko,[c] John M. Kelly[c] and Margaret E. Brennan-Fournet*[ad]

A rapid, wash-free highly sensitive detection method for C-reactive protein (hs-CRP) is reported with both triangular silver nanoplate (TSNP) and Au-edge coated TSNP biosensor sols. The latter shows higher assay sensitivity as well as excellent stability under assay conditions including centrifugation and salinity. A series of Au derived TSNP sols including Au-edge-coated TSNP, AuAg nanomesh and nanobox derived sols are examined as statistically representative saline-stable enhanced ensemble local surface plasmon resonance (LSPR) refractive index sensitive sensors. Samples with plasmon bands spanning the biological spectral window are prepared showing enhancement compared with the original TSNP sols. Refractive index sensitivities as high as 1816 nm RIU^{-1} are exhibited by Au-edge-coated TSNP sols. The priority of ensemble refractive index sensitivity values over figures of merit in characterising these sols is examined using discrete dipole approximation calculations and single nanostructure dark field microscopy measurements. We anticipate that the high ensemble LSPR refractive index sensitivities, saline stability and ultra-low detection limit capacity of the Au derived TSNP sols, in particular Au-edge coated TSNP sols, present them as excellent candidates for sensing within biological environments.

A Introduction

Recently there has been rapidly growing interest in using noble metallic nanostructures with refractive index sensitive LSPR as signal transducers in biosensing applications.[1,2] Refractive index sensitive LSPR nanostructures can exhibit systematic LSPR shifts upon the binding of analyte molecules which induce changes in the local refractive index at the nanostructure's surface. A wide range of nanostructures exhibiting high linear refractive index sensitivities, $\Delta\lambda/\Delta n$ (nm RIU^{-1}), have been reported to date including triangular silver nanoplates,[3] edge gold coated silver nanoprisms,[4] nanorice,[5] nanobipyramids,[6] and nanorings.[7] Factors including the relatively high refractive index of proteins ($\sim$1.5) the short electromagnetic field decay length of LSPR ($\sim$20 nm), which is on the same size scale as proteins, are among the benefits of using highly refractive index sensitive nanostructures for probing protein interactions.[8]

Although a broad range of highly sensitive nanostructures have been presented and proposed for biological recognition sensing applications, challenges remain in attaining the parameters and properties essential for clinically relevant biosensing. It is critical that nanostructure geometric and optical properties, in particular their high LSPR refractive index sensitivities are retained under physiological conditions. In the clinical setting, methods which provide statistically significant data are essential. However, given the many existing challenges in the synthesis of homogenous ensembles of complex shaped nanostructures capable of high LSPR refractive index sensitivities, the focus to date has mainly been on the examination of individually probed, immobilized nanostructures.[8,9] This emphasizes the importance in developing arrays or ensembles of nanostructure biosensors with high geometric and optical uniformity which exhibit high ensemble LSPR sensitivities.

In the clinical setting, the evaluation of inflammatory diseases, patient response to therapies and cardiovascular disease risk would be greatly facilitated by a rapid, straightforward method of measuring C-reactive protein, (CRP), an acute phase marker for inflammation, infection or tissue injury.[10,11] Cardiovascular diseases including, myocardial infarction, myocardial ischemia and unstable angina result in increased CRP levels.[12,13] Studies have shown raised levels of CRP correlate

[a]*School of Physics, National University of Ireland, Galway, Ireland. E-mail: Tess.Mahoneynuigalway.ie; Tel: +353 91 492490*

[b]*School of Physics, Trinity College Dublin, Dublin 2, Ireland. E-mail: physics@tcd.ie; Tel: +353-(0)1-896 4141*

[c]*School of Chemistry, Trinity College Dublin, Dublin 2, Ireland. E-mail: galvinji@tcd.ie; Tel: +353 (0) 1 896 2040*

[d]*Department of Bioelectronics, Ecole Nationale Superieure des Mines, CMP-EMSE, MOC, 880 Rue de Mimet, Gardanne 13541, France. E-mail: malliaras@emse.fr; Tel: +33 (0)4 42 61 66 44*

strongly with the potential development of coronary heart disease, its prognosis and severity.[14–16] The American Heart Association reports that hs-CRP levels of < 1 mg L^{-1}, 1 mg L^{-1} to 3 mg L^{-1} or > 3 mg L^{-1} correspond to low, average or high risk of cardiovascular disease development, respectively.[17]

Nanostructure biosensors which are not immobilised to a substrate are advantageous, as they are homogenously in phase with the target analyte, support biomolecular recognition kinetics and have their total surface area available for interaction without the influence of substrate coupling. In the clinical setting assays which are wash free have a considerable advantage over other assays, saving on time, complexity and cost. Here, we present Triangular Silver Nanoplate (TSNP) and gold derivatised TSNP sols for the novel one-step rapid detection of CRP with excellent sensitivity.

Previously we have presented TSNP sols which have high geometric uniformity, exhibit versatile optical tunability,[18] and display high ensemble refractive index sensitivities.[3] These high ensemble refractive index sensitivities lie along the maximum values predicted by Miller and Lazarides for arbitrary nanostructures with LSPR dipole peak wavelengths (λ_{max}) positioned up to 800 nm.[19] The optical parameters of these TSNP nanostructures have been found to be directly proportional to their high aspect ratios which localizes and enhances the electromagnetic field at the nanoplate's surface.[3] We have previously reported that this localization allows for the continued scaling of the high ensemble LSPR refractive index sensitivities, even at edge lengths larger than 200 nm.[20] In addition to their highly sensitive response, the ensemble status of these TSNP sols provide a system to generate statistically relevant sensing data, homogeneously in phase with the potential target biomolecule of interest.

Unprotected TSNPs are known to be subject to degradation or etching under physiological conditions by catalytic oxidation of the silver surface due to the presence of chloride ions.[21] Such etching can lead to alteration of the geometrical and structural characteristics of the silver nanoparticles normally causing a substantial blue shift and impairing their plasmonic resonance properties.[22] Various coating approaches can be used to achieve protection of silver surfaces, however challenges remain in preserving the plasmonic response in protected silver nanostructures.[23–25] We have reported preliminary work on the successful preparation of Au-edge-coated TSNP sols with optical tunability limited to the visible range.[26] These sols have increased stability towards chloride etching and retain high ensemble refractive index sensitivities within the visible spectral range.

In this manuscript we report the development of a rapid, wash-free highly sensitive detection method for C-reactive protein (hs-CRP) with both the TSNPs and the Au-edge coated TSNP biosensor sols. The Au-edge coated TSNP CRP sensors show detection levels as low as 3.3×10^{-3} mg L^{-1}, which is several orders of magnitude below the detection range recommended by the American Heart Association, illustrating the potential of Au derivatised TSNP sols to provide enhanced biosensor sensitivity. Investigations of new Au derivatised TSNP sols are carried out in order to explain the improved

performance of the Au edge coated TSNP sensors and to explore the potential for the further enhancement of sensing sensitivity and performance. We examine how through modification of the basic nanoplate structure, the ensemble LSPR refractive index sensitivities may be enhanced above those of the original TSNP, exceeding the maximum values achievable by arbitrary nanostructures predicted by Miller and Lazarides.[19] New Au-edge-coated TSNP sols with LSPR at near infrared wavelengths at the edge of the biological spectral window are reported. These AuTSNP exhibit ensemble refractive index sensitivities as high as 1816 nm RIU^{-1}, exceeding those previously reported for other nanostructures at similar LSPR λ_{max}. The Au-edge-coating method, which utilizes galvanic replacement processes, is directed to synthesise more complex nanostructures including AuAg TSNP derived nanomesh and nanobox sols.[27] These nanobox and nanomesh sols provide key information on the roles of features such as electromagnetic field hot-spots, nanostructure thickness and the full width half maximum (FWHM) in enhancing the refractive index sensitivity above that of the original TSNP sols. The use of the sensing figure of merit (FOM) {defined as the nanostructure linear refractive index sensitivity $\Delta\lambda/\Delta n$ (nm RIU^{-1}) divided by the FWHM of the LSPR resonance peak} as introduced by Sherry et al.[28] is examined for these ensembles. Dark field microscopy is used to compare ensemble and single nanostructure refractive index sensitivities. The spectral location of the LSPR λ_{max} within the tissue and water absorption window, their enhanced high ensemble sensitivities, saline stability and above all their demonstration for rapid straightforward highly sensitive assays suggests the Au derived TSNP sols to be excellent candidates for biosensing applications and clinical screening tools.

B Experimental and materials

Reagents and materials

Reagents were obtained from Sigma-Aldrich and used as received. Triangular Silver Nanoplate (TSNP) sols were prepared using the silver seed-catalyzed reduction of AgNO$_3$ previously described.[13] The process involves combining 5 mL distilled water, aqueous ascorbic acid (75 μL, 10 mM) and various quantities of seed solution (see Table 1), followed by addition of 3 mL aqueous AgNO$_3$ (0.5 mM) at a rate of 1 mL min^{-1} in a process that take 3 to 10 minutes. The resulting spectra are shown in Fig. 1a and their LSPR λ_{max} are recorded in Table 1.

Au-edge-coated TSNP synthesis

Au-edge-coated TSNP were synthesized from TSNPs prepared as in the previous section using a previously reported method.[26] A thin coating of gold is applied onto the edges of the nanoplates by adding 150 μL of 10 mM ascorbic acid to the TSNP solution and adding an appropriate volume of chloroauric acid (HAuCl$_4$) with a syringe pump at a rate of 0.2 mL min^{-1}, while stirring the solution (Fig. 1a and Table 1). The volume of 0.5 M HAuCl$_4$ solution required to produce the Au-edge-coating onto the TSNP was calculated in accordance with the total TSNP nanostructure edge surface area and concentration within each sample

Table 1 Characteristic parameters of Au-edge coated TSNP nanostructure sols

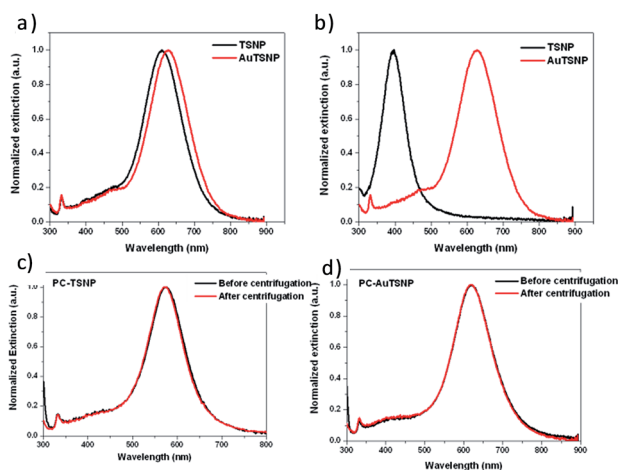| Original TSNP λ_{max} (nm)	Seed volume (μL)	Ag : Au molar ratio	HAuCl$_4$ (μL)	Au edged TSNP λ_{max} (nm)	$\Delta\lambda/\Delta n$ (nm RIU^{-1})	FWHM (nm)	FOM (RIU^{-1})
600	200	1 : 0.073	220	628	358	188	1.9
680	150	1 : 0.052	155	699	378	207	1.8
730	100	1 : 0.041	122	737	448	165	2.7
805	50	1 : 0.03	90	814	463	180	2.6
846	25	1 : 0.025	75	862	624	240	2.6
847	20	1 : 0.022	65	865	619	392	1.6
855	15	1 : 0.025	75	882	527	207	2.6
903	10	1 : 0.02	60	912	759	249	3.1
907	8	1 : 0.02	60	946	981	241	4.1
917	5	1 : 0.02	70	1041	1082	352	3.1
1091	4	1 : 0.027	80	1111	1123	310	3.6
1111	3	1 : 0.027	80	1155	1266	349	3.6
1132	2	1 : 0.027	80	1167	1128	387	2.9
1167	1	1 : 0.013	40	1185	1816	331	5.5

Fig. 1 UV-vis spectra of (a) a TSNP sol and the AuTSNP sol derived from it; (b) the same sols placed in 10 mM NaCl for 5 min. UV-vis spectra before (black curve) and after (red curve) centrifugation (c) PC-TSNP, (d) PC-AuTSNP.

volume. The accuracy of these calculations was confirmed by the spectroscopic stability of the LSPR λ_{max}.

AuAg nanomesh and nanobox synthesis

AuAg nanomesh and nanobox sols were derived from TSNP sols synthesized using previously reported methods.[18,27] A batch of TSNP was fabricated by adding 800 μL of the seed solution and 600 μL of 10 mM ascorbic acid to 40 mL of Millipore water followed by of 24 mL of 0.5 mM AgNO$_3$ at a rate of 5 mL min^{-1} through a syringe pump. No trisodium citrate (TSC) was added to the Ag nanoplate solution after growth. The Ag nanoplate solution was split into 8 equal volumes with one eighth left as the control Ag nanoplate sample. Appropriate amounts of ascorbic acid were then added to the remaining 7 volumes followed by corresponding amounts of 0.5 mM HAuCl$_4$ by syringe pump at a rate of 1 mL min^{-1}. The following volumes of HAuCl$_4$ were used for the particular samples: (A) 0 mL, (B) 0.5 mL, (C)

1.0 mL, (D) 2.0 mL, (E) 4.0 mL, (F) 6.0 mL, (G) 8.0 mL, (H) 10.0 mL. These were used with the following corresponding volumes of ascorbic acid: (A) 0 μL, (B) 150 μL, (C) 150 μL, (D) 225 μL, (E) 375 μL, (F) 525 μL, (G) 675 μL, (H) 825 μL (see Table 2).

One-pot synthesis of TSNP and AuTSNP CRP biosensors

TSNP and Au-edge-coated TSNP biosensors are prepared using a one-pot synthesis which does not involve any additional conjugation steps. Here, cytidine 5′-diphosphocholine (PC), which has a high affinity for CRP in the presence of calcium is used as the receptor agent. Each subunit of the CRP pentamer can bind a single PC molecule *via* the choline group, cooperating with the two CRP-bound calcium ions *via* the phosphate group.[29]

TSNP and Au-edge coated TSNP sols were synthesized as before with the omission of the addition of TSC at the end of the growth step. Appropriate volumes of 0.1 M PC were added to each sol. The mixture solutions were incubated for 30 min at 4°, followed by addition of aqueous TSC (25 mM) for further stabilization. The final concentration for PC and TSC was 5 mM and 0.3 mM, respectively. The sols were then incubated overnight at 4° in the dark. Prior to use, aliquots of prepared PC-functionalized TSNP (PC-TSNP) and AuTSNP (PC-AuTSNP) were centrifuged at 13 000 rpm and 4° for 30 min. The supernatant was removed and the pellet was redispersed to 10% of initial

Table 2 Characteristic parameters of AuAg nanomesh and nanobox TSNP nanostructure sols

Sample	λ_{max} (nm)	Ag : Au molar ratio	$\Delta\lambda/\Delta n$ (nm RIU^{-1})	FWHM (nm)	FOM (RIU^{-1})
B	675	1 : 0.17	314	143	2.19
C	708	1 : 0.34	530	310	1.71
D	711	1 : 0.67	381	227	1.68
E	742	1 : 1.34	407	228	1.78
F	789	1 : 2.01	431	226	1.91
G	795	1 : 2.34	610	328	1.86
H	843	1 : 3.35	598	376	1.59

volume in water. The refractive index sensitivities of the two CRP biosensor sols were measured using the sucrose solution method described below.

One-step, wash-free highly sensitive rapid detection of C-reactive protein

Straightforward and rapid hs-CRP assays were performed in disposable UV micro cuvettes (BRAND) without washing and characterized using a fiber optic spectrometer (Ocean Optics). In a typical assay, human CRP (1 μL) at various concentrations in phosphate buffer (PB; 10 mM, pH 6.5) were added to PC-TSNP/PC-AuTSNP (10 μL) in 279 μL of water and 10 μL, 1 mM CaCl$_2$. The final concentration of CRP ranged from 0 to 3.34 mg L^{-1} and UV-vis spectra were recorded at each concentration after 3 minutes.

Saline stability analysis

Each of the TSNP derived sols were tested for stability against etching by chloride by exposing the nanoparticles to the presence of 10 mM NaCl. These samples were prepared by mixing equal volumes of TSNP derived sol and 20 mM NaCl solution. UV-Vis spectra were taken at various time intervals to monitor the stability of the λ_{max} of the samples.

LSPR refractive index sensitivity

The LSPR refractive index sensitivity of each sol was determined by suspending the sol in sucrose prepared in Millipore water at concentrations of 10 wt%, 25 wt% and 50 wt%. A volume of the TSNP sol was then mixed in with a certain volume of the sucrose solutions and the corresponding refractive index of the solution mixture surrounding the nanoplates was calculated using the Lorentz–Lorentz equation, where

$$\frac{n_{12}^2-1}{n_{12}^2-2} = \varphi_1 \frac{n_1^2-1}{n_1^1+2} + \varphi_2 \frac{n_2^2-1}{n_2^2+2}$$

where n_{12} is the refractive index of the mixture, n_1 and φ_1 are the refractive index and volume fraction of the nanoparticle sols and n_2 and φ_2 are the refractive index and the volume fraction of the sucrose concentration. The solution phase ensemble extinction spectra of the nanostructure sols suspended in the different sucrose solutions were acquired on a Cary-Varian NIR spectrometer. The sensitivity of the solution phase nanostructures $\Delta\lambda_{max}/\Delta n$ (nm RIU^{-1}) was calculated by plotting the shift observed in the peak LSPR wavelength $\Delta\lambda_{max}$ against the corresponding refractive index of the sucrose.

Dark field sample preparation

Dark Field Microscopy samples were prepared using both Fisher and Menzel brand glass slides of 1 mm thickness, with the Fisher Brand being most commonly used throughout these studies. Samples were sandwiched within a securely sealed spacer between the glass slides and a Fisher brand coverslip of No. 1 thickness (0.13–0.16 mm). The sample spacers used were Sigma Secure-Seal Imaging spacers with a 9 mm diameter and

0.12 mm thickness. 5 μl of sample was dropped using a micropipette within the spacer chamber.

Instrumentation

UV-Vis-NIR spectra were performed on a Cary 6000i UV-Vis-NIR double beam spectrometer. TEM images were taken on a JEOL JEM-2100 LaB6 TEM operating at 200 keV. Dark Field spectroscopy was performed on an Olympus IX81 transmission microscope using an IX2-TLW water immersed dark field condenser lens with a numerical aperture (N.A.) of 0.9, an oil immersed objective with a N.A. of 1.3 and a 100 W Halogen light source to illuminate the sample. Olympus immersion oil type F with a refractive index of 1.518 was used for the oil immersed objective. Dark Field spectra were acquired using a Princeton Instruments Acton Series SpectroPro-2300i with a focal length of 300 nm and a triple grating turret which is connected to a Pixis 256 CCD camera with a 1024 × 256 pixel array format, 6.7 mm height.

C   Results

Nanoparticle synthesis and characterization

Triangular silver nanoplates with edge lengths varying from 25 nm to 200 nm (and hence LSPR λ_{max} from *ca.* 600 nm to 1197 nm), were prepared using a silver seed-catalyzed reduction of AgNO$_3$ (Fig. 1a).[18] The LSPR λ_{max} is determined by the ratio of Ag$^+$ to seed and results in red shifts from the visible to NIR wavelengths upon decreasing the volumes of seed solutions.

The Au edge-coating process uses gold salt in small quantities and high concentrations of ascorbic acid to aid in the reduction of AuCl$_4$ to inhibit the oxidation of silver at the surface of the nanoplate.[26] As galvanic replacement is minimized, epitaxial deposition of a thin layer of gold onto the edges of the TSNP occurs. AuAg TSNP nanomesh and nanobox sols are synthesised through the controlled direction of the galvanic replacement process.

UV-vis spectra of a typical TSNP sol and the AuTSNP sol prepared from it are shown in Fig. 1a. The gold coating results in a 18 nm red shift in the LSPR peak from 609 nm to 627 nm and a slight broadening of the band. In the presence of saline (Fig. 1b), no shift in the LSPR peak is observed for the AuTSNP sample whereas the LSPR peak of TSNP sol blueshifts to 397 nm due to Cl$^-$ etching.

Highly sensitive C-reactive protein detection using TSNP and Au-edge-coated TSNP

As discussed in the Introduction, increased CRP levels are found in patients with cardiovascular disease.[12,13]

In the current work a rapid single step CRP sensing method has been developed using cytidine 5′-diphosphocholine (PC) coated TSNP (PC-TSNP) and PC-AuTSNP sols involving direct-binding and without requiring washing as depicted in the schematic in Fig. 2a. UV-Vis spectra of PC-TSNP/PC-AuTNSP sols were taken before and 3 min after the addition of the analyte. It may be noted that upon PC functionalization, TSNP and AuTSNP are found to typically exhibit 7 and 9 nm red shifts
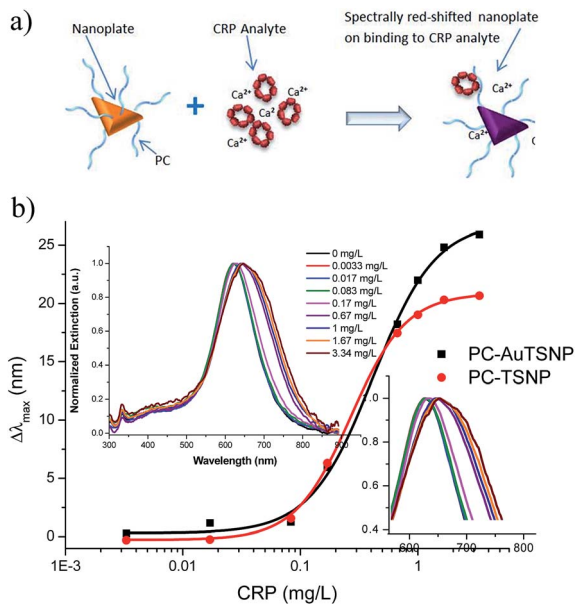
Fig. 2 (a) Schematic showing the CRP assay, where PC functionalised nanoplates bind to CRP in the presence of Ca^{2+} ions resulting in a spectral shift due to the increased local refractive index. (b) Dose response curve for LSPR peak shift (±1 nm) as a function of the CRP concentration for PC-AuTSNP (black) and PC-TSNP (red). Insets: above: UV-Vis spectra of PC-AuTSNP in the presence of CRP concentrations from 0 to 3.34 mg L^{-1}, below: enlarged spectral peaks of the PC-AuTSNP in the presence of CRP concentrations from 0 to 3.34 mg L^{-1}.

in their peak wavelengths due to the adsorption of PC onto their surfaces.

Both the PC-TSNP and PC-AuTSNP sols show high stability under centrifugation which is required to remove the excess PC ligand. The PC-AuTSNP undergoes no detectable wavelength shift, (Fig. 1d) while there is a very slight blue shift (of the order of 1 to 2 nm) of the PC-TSNP (Fig. 1c), indicating the increased robustness of Au derived sensor sol.

Detection of very low hs-CRP concentrations were found for both PC-TSNP and PC-AuTSNP sensor sols as shown in dose curve responses in Fig. 2b. However the PC-AuTSNP show an increased overall LSPR peak red wavelength shift compared with the PC-TSNP. Additionally at very low concentrations of CRP (below 0.017 mg L^{-1}) very small blueshifts are observed for the PC-TSNP, which may be attributed to the etching of the nanoplates by Cl^- ions from $CaCl_2$ solution used in this assay to facilitate PC-CRP binding which is Ca^{2+} dependent. No such blue shift is observed in the assay using PC-AuTSNP. Instead the diagnostic red shift is detected at CRP levels as low as 3.3×10^{-3} mg L^{-1} (inset Fig. 2). This again illustrates the superior qualities provided by the protection by the gold coating at the edges of the nanostructures which allows the extension of the limit of detection for these biosensors.

To further explore the applicability of these Au-coated TSNPs we have prepared a range of edge-coated samples with differing edge size, as well as nanostructures with a higher gold content which have nanomesh and nanobox morphologies. In each case we test the saline stability and the refractive index sensitivity using a sucrose-assay.

Au-edge-coated TSNPs of different edge length

The amenability of the previously described Au edge-coating method[26] to broad spectral tunability was examined by applying it to the prepared TSNP sols (Table 1). Fig. 3b shows an example of a TEM image of Au-edge-coated TSNPs and a schematic highlighting the Au coating of the edges of a TSNP. The success of the Au-edge coating method for the various sized TSNP sols was determined by examining the amount of gold needed to give the TSNP resistance to chloride etching in saline solutions. This was readily monitored, as in the presence of salt the TSNP plasmon band shifts to shorter wavelengths (Fig. 1a and b), as etching occurs.

A similar experiment was performed by adding the AuTSNP sols to 10 mM NaCl solution. The corresponding extinction spectra were recorded after approximately 5 min. Samples which displayed only a small red-shift in their LSPR λ_{max} or which did not shift were regarded as exhibiting successful coatings for the concentration of $HAuCl_4$ employed. As expected, less $HAuCl_4$ is needed to protect the larger edged TSNPs against etching (Fig. 3c), attributable to a decrease in TSNP edge surface area present because of the smaller number of TSNPs in the solution.[18] Fig. 3d displays the resultant spectra of the saline stable, optically tunable Au-edge-coated TSNP sols highlighting their merit for biological TSNP sols applications across the biological spectral window.

AuAg TSNP nanomesh and nanobox sols

While galvanic replacement is deliberately minimised in the Au-edge-coating process, it is however useful in the synthesis of the
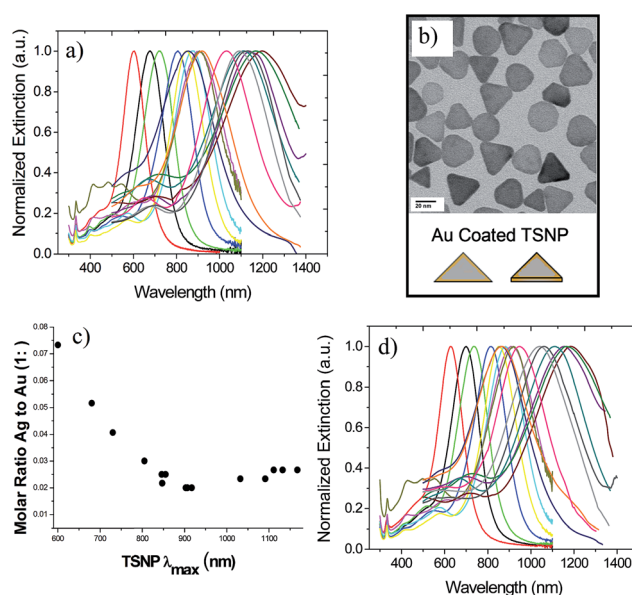

Fig. 3 (a) Extinction spectra of the original TSNP, (b) TEM image and schematic diagram of Au-edge-coated TSNP with a LSPR λ_{max} at 907 nm, (c) the molar ratio of Au : Ag required to successfully stabilize the TSNP sols against etching by coating the edges with gold, for each sample across the visible to NIR spectral region and (d) the resultant LSPR spectra for the Au-edge-coated TSNPs.

more complex nanomesh and nanobox structures. AuAg nanomesh and nanobox derivatives of TSNP sols were synthesized using the protocol as previously described by Aherne *et al.*[27] A series of samples (labelled A-H) were prepared by adding increasing amounts of $HAuCl_4$ in the presence of corresponding volumes of ascorbic acid to aliquots of a TSNP sol of LSPR λ_{max} of 725 nm and edge length of 35 nm, to create nanomesh and nanobox structures given in Table 2.

For earlier nanostructures of the series (corresponding to lower amounts of added gold), mesh like structures which have hollow features within the TSNP structure were observed (Fig. 4a). The hollows are created by oxidation of the Ag by the $AuCl_4^-$ ions by galvanic replacement despite the presence of ascorbic acid. As the stages of the series progress and more $HAuCl_4$ and ascorbic acid is added, there is a co-reduction of Ag^+ and $AuCl_4^-$ to form an alloy and the alloy layer grows towards the centre of the nanostructure closing it up as the reaction proceeds.

This forms a complete AuAg alloy shell with a hollow interior which increases in thickness as more Au is added (Fig. 4b). The LSPR spectra of the series of AuAg nanomesh and nanobox sols at the various stages of growth (A to H) are shown in Fig. 4c. The plasmonic resonance properties of these nanostructures evolve from the original TSNP with a red shift in the LSPR λ_{max} observed for the earlier stages of growth of the nanomesh structures while a blue shift is observed at the later stages of growth as the nanobox structures are formed.

The stability of these more intricate nanostructures against etching by chloride (Fig. 4d) is an important characteristic in determining the basis for their merit for biosensing applications. As shown above, unprotected TSNPs (sample A), undergo an immediate large blue shift of the LSPR λ_{max} upon addition of 10 mM NaCl (Fig. 4d). No such blue shift is found for samples B

to H due to their resistance to the chloride etching due to the reduction of the Au onto the surface of the nanostructure at the earlier stages of growth and the formation of a more stable AuAg alloy at the later stages of growth. In general a small red shift is observed and the spectrum remains stable for several days in the salt solution.

Ensemble LSPR refractive index sensitivities

The ensemble LSPR refractive index sensitivities of each of the TSNP and Au derived TSNP sols and their PC functionalised CRP sensors were measured using sucrose solutions of different concentrations with corresponding varying refractive index.

While the sensitivities of all as-prepared and centrifuged samples exceed the maximum values predicted by the theory of Miller *et al.*[19] (Fig. 5), both AuTSNP and the PC-AuTSNP present higher sensitivities and stabilities upon centrifugation. The relative performance of the sensors in the CRP assays can be directly related to their sensitivity measurements. Corresponding with the assay results the higher refractive sensitivity value measured for the PC-AuTSNP of 336 nm RIU^{-1} which has a λ_{max} of 618 nm, compared to 269 nm RIU^{-1} for the PC-TSNP which has a λ_{max} at 572 nm, contributes to and the larger wavelength shift measured in response to the CRP binding and their increased detection sensitivity. These results indicate that the Au edge coating of the TSNPs is effective in contributing to the potential of these sols to serve as robust and highly sensitive biosensors for detection of CRP.

Au-edge-coated TSNP sensitivities were measured to range from 358 nm RIU^{-1} at a LSPR λ_{max} of 628 nm up to a maximum of 1816 nm RIU^{-1} at a LSPR λ_{max} of 1197 nm (Fig. 6a). The highest values recorded for these Au-edge-coated TSNP sols exceed values previously reported for other nanostructures at similar LSPR λ_{max}, including those for single nanostructures (1060 nm RIU^{-1} for hematite core/Au shell nanorice at LSPR λ_{max} of 1160 nm,[5] and 880 nm RIU^{-1} measured for Au nanorings with a λ_{max} of 1545 nm).[6] The Miller predicted values were calculated at the various wavelengths up to the maximum of 800 nm using their wavelength dependent theory.[19]

Upon comparing the LSPR refractive index sensitivities of the Au-edge-coated TSNP sols to values recorded for the bare TSNP sols,[3] it is clear that the sensitivities of both follow a similar trend up to wavelengths of 900 nm and lie along the Miller and Lazarides trend. At longer wavelengths the Au-edge-
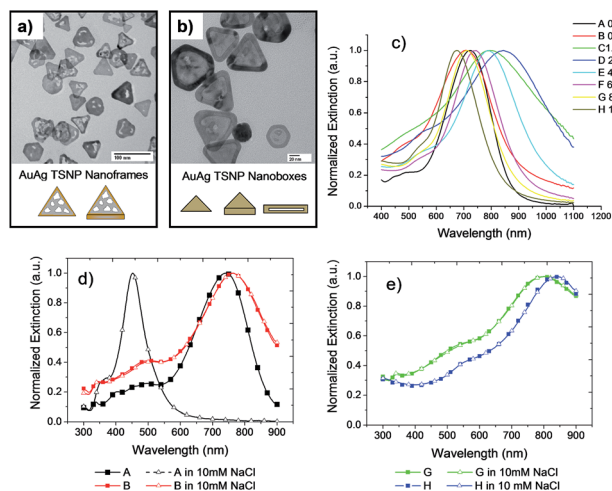

Fig. 4 TEM image and schematic of (a) TSNP derived nanomeshs and (b) TSNP derived AuAg nanoboxes. (c) UV-Vis spectra of the TSNP derived nanomeshes (B), (C) and (D) and nanoboxes (G) and (H) highlighting the transition of the LSPR λ_{max} as the various stages of growth progress. (d) UV-vis spectra indicating the stability of the LSPR λ_{max} of representative bare TSNP (A) and the earliest derived nanomesh (B) and (e) nanobox samples (G) and (H) upon exposure to 10 mM NaCl.
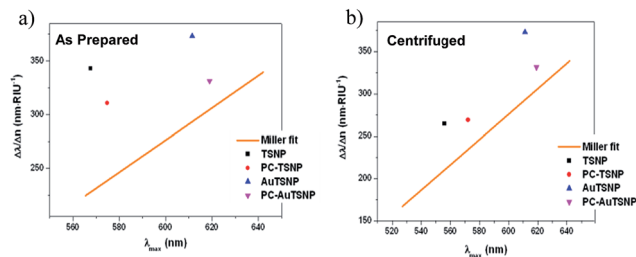

Fig. 5 Comparison of experimental ensemble LSPR sensitivities of the TSNP, the PC functionalised TSNP, AuTSNP and PC functionalised AuTSNP, as-prepared sols (A) and centrifuged sols (B) to the Miller line.
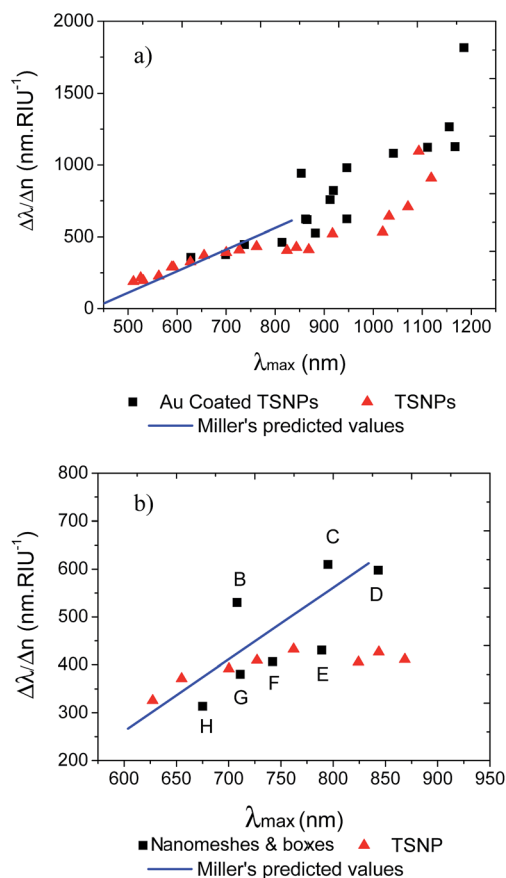
Fig. 6 LSPR linear refractive index sensitivities compared to original uncoated TSNP sols and Miller and Lazarides predicted values for (a) the Au-edge-coated TSNP sols and (b) the AuAg nanomesh and nanobox sols.

and ascorbic acid at these stages of growth results in the formation of an alloy layer. The AuAg alloy layer increases in thickness as more Au is added completely covering the interior. Samples E to H are accompanied by a blue-shift in the LSPR λ_{max} and a reduction in the FWHM as the uniformity of the nanostructures is improved with the filling in of the pores. These results show that samples with modified morphologies and composition can exhibit quite different sensitivities while having similar λ_{max} and overall geometries (compare samples B and G or samples C and E). These studies verify that ensemble LSPR sensitivities are not exclusively dependent upon the position of the LSPR λ_{max} and that the sensitivity can be increased by control over the morphology of the nanoparticles with important implications for the optimisation of their performance for biosensing.

Dark field studies of individual TSNP nanoplates

Using dark field microscopy, FWHM values for single individual TSNP were measured.

These experimental values compare closely with single TSNP FWHM calculated using the discrete dipole approximation (DDA) method (Fig. 7a). Experimentally measured ensemble TSNP sols refractive index sensitivities were found to also coincide with the values determined using DDA for single TSNP demonstrating minimal diminution in these values due to

coated TSNP sol ensemble sensitivities are observed to be greater than those of the original TSNPs and follow a linear trend corresponding to that of an NIR extrapolated Miller trend. This enhancement at longer wavelengths is possibly associated with increased surface polarization and local electric field strength due to the presence of the Au edge coating and the gold silver interface. This marked increase in sensitivity enhancement coincides with nanoplate sizes reaching and going beyond that of the electron mean free path which is of the order 50 nm.

For the nanomesh and nanobox samples the ensemble LSPR refractive index sensitivities for nanostructures B and C is observed to be significantly above that which is predicted theoretically for arbitrary nanostructures (Fig. 6b). This increased sensitivity corresponds to the porous nanomesh type structures that occur during these early stages of growth as a result of the oxidation of the Ag by the $AuCl_4^-$ ions. The enhanced sensitivities of the nanomesh sols B and C are significantly higher than those for basic TSNP sols with the same LSPR λ_{max} which we attribute to the presence of additional electromagnetic field components in the vicinity of the pores.

By contrast the ensemble LSPR sensitivities are substantially less for nanobox samples E to H. In these nanostructures the pores have become closed over as the presence of more $HAuCl_4$
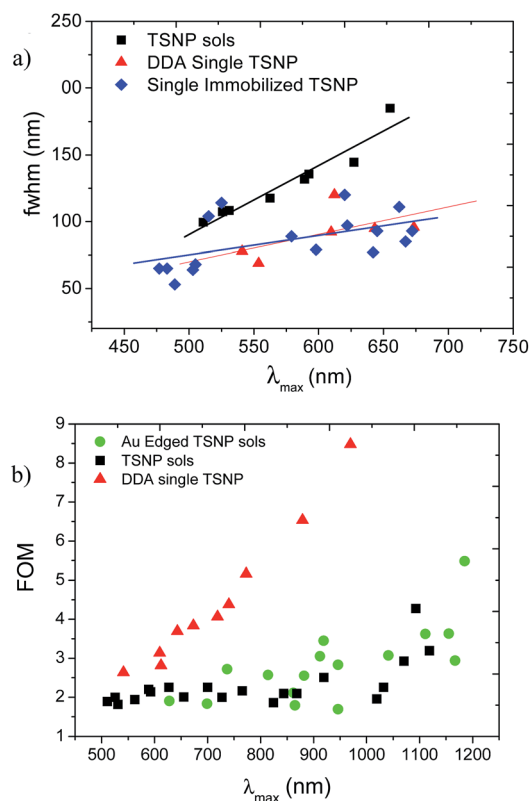

Fig. 7 (a) FWHM values for the spectra of original ensemble TSNP sols, calculated single TSNP and darkfield measured single TSNP (b) FOM values for Au-edge-coated TSNP sols compared to TSNP sols and calculated single TSNP.

averaging effects and highlighting the benefits of their high geometrically uniformity and their real potential for statistically representative biosensors.

The conventional Figure of Merit (FOM) used within the literature for the comparison of the sensing capabilities of plasmonic nanostructures considers the ratio of the LSPR refractive index sensitivity to the FWHM of the spectral resonance.[28] The FWHM of calculated single TSNP range between 60 nm and 120 nm compared with 100 nm to 190 nm over the same wavelength range for the TSNP ensembles. The differences in the FWHM means that the calculated FOM values for the single TSNP are notably higher that that of the ensemble TSNP (Fig. 7a). Importantly we record a maximum FOM of 5.48 for an Au-edge-coated TSNP sol with a LSPR λ_{max} of 1197 nm (Fig. 7b). This is the highest value recorded for ensemble solution phase nanostructures to date and is comparable to single nanostructure values such as 5.4 for single silver nanocubes,[28] and 5.7 for gold nanoclusters.[33]

D   Discussion

High refractive index sensitive sols for one-step wash-free rapid assays with ultra low detection limits

The rapid one-step wash-free hs-CRP assays with ultra low detection capacities demonstrate the effective translation of these high refractive index sensitive sols for biosensing. The Au-edge coated TSNP sol shows higher stability and sensitivity over the original TSNP sol, with a red shift in the LSPR peak of PC-AuTSNP detectable for CRP concentrations as low as 3.3×10^{-3} mg L^{-1}. (Fig. 2 red curve). The enhanced sensitivity and saline stability of the AuTSNP over the TSNP sensor sols can be directly associated with the increased refractive index sensitivity of the AuTSNP and their effective retention of that sensitivity under assay centrifugation conditions. The dynamic range and sensitivity of the assay can be adjusted by varying the quantities of biosensors used and the size of the nanoplates used for preparing the biosensors. This technique is applicable to numerous protein tests and holds the promise of simple and rapid label-free bioassays with excellent sensitivity.

Enhancement in ensemble LSPR sensitivities

On comparison with the ensemble LSPR refractive index sensitivities of the original TSNP sols, Au-edge-coated TSNP sol sensitivities are observed to be equivalently high at visible wavelengths and exceed the TSNP sol values at NIR wavelengths. Such sensitivity enhancements have been reported previously for modified nanostructures with increased complexity. For example complex nanostructures such as rod-shaped nanorattles have been synthesized from nanorods using a galvanic replacement step.[30] Similarly Au nanorings were fabricated from Au nanodisks using various depositions and argon ion beam etching steps.[6] In both of these particular studies the derived complex nanostructures displayed higher refractive index sensitivities compared to the template solid nanorods and nanodisks respectively. The oxidation of the Ag by the AuCl$_4^-$ ions within the synthesis of such more complex

nanostructures may result in the formation of numerous small localized, enhanced electromagnetic fields or "hot spots" within the nanostructure. Mahmoud et al. have previously shown that the plasmon field strength of a hollow nanostructure is increased greatly over that of a solid nanostructure of comparable dimensions.[31] This increase is attributed to the coupling between the external and internal surface electric fields within the hollow nanostructures which is shown to be directly related to the resultant refractive index sensitivity.[32] Therefore coupling between the numerous hollows observed within the AuAg nanomeshes may lead to greatly increased plasmon field strengths, resulting in sensitivity enhancement. The reduction in sensitivity observed for AuAg series of sols at the later stages of the series, (E to G), may be attributed to the closure of the hollow features as the galvanic replacement process is increased. Furthermore, Sample H (nanobox) has a sensitivity that is below what would be expected for an original TSNP sol of the same λ_{max}. Note however that previous studies have shown that the nanoplates grown to the stage of sample H have twice the thickness of the original template TSNP.[27] For example on growing a TSNP sol with average nanoplate thickness of 7 ± 1 nm to form an AuAg nanobox sol at the stage of sample H the thickness will have increased to 15 ± 2 nm.[27] This thickening decreases the aspect ratio resulting in an expected reduction in refractive index sensitivity,[3,20] even though there is no significant LSPR λ_{max} change. This result provides further evidence for the aspect ratio dependence of the LSPR refractive index sensitivity, independent of the LSPR λ_{max} spectral location.

Comparing the sensing figure of merit between ensemble and single nanostructures

Considering the challenges in synthesizing ensembles of complex shaped nanostructures with high homogeneity,[9] to date the FOM has more generally been applied to single and individual nanostructures. The maximum FOM values reported to date are those of 10.7 for single gold nanostars,[34] and 23.3 for finite gold nanohole arrays.[35] Both of these nanostructures displayed extremely narrow spectral resonances which greatly increased the FOM placing significant emphasis on the higher resolution of the measurable LSPR shift, notwithstanding the modest values recorded for their refractive index sensitivity. In the case of the AuAg nanomeshes and nanoboxes, the high ensemble refractive index sensitivities recorded in conjunction with their high stability to chloride etching would suggest that these nanostructure sols would be a most proficient signal transducer for biosensing applications. However, random positioning of the pore features within these nanostructures during the galvanic replacement process increases the geometric distribution within the sols to a certain degree, leading to further inhomogeneous broadening of the LSPR linewidth resulting in FWHM in the range of 300 nm. Conventional FOM calculations would result therefore in values below 2 for AuAg nanomesh and nanobox sol ensembles which are significantly lower than those of the original TSNP sols.[3]

Single TSNP exhibit narrow FWHM resulting in a significant FOM increase over those of the TSNP sols, with values as high as

8.5 (Fig. 7), even though the LSRP refractive index sensitivities are equivalent. Although single nanostructures can provide higher FOMs, their practical application is limited due to the restriction to individual readings and the requirement of more elaborate read out techniques such as dark field spectroscopy. While the FWHM of Au derived TSNP sols may be reduced with synthesis advancements to further improve geometric uniformity, their limitations of low FOM is greatly outweighed by their advantages of saline stability and statistically representative data from their high ensemble LSRP refractive index sensitivities. This is underlined by the demonstration of higher hs-CRP detection sensitivities for PC-AuTSNP (FOM = 2.8, refractive index sensitivity = 336 nm RIU^{-1}) than PC-TSNP (FOM = 3.2, refractive index sensitivity = 269 nm RIU^{-1}) indicating the priority of refractive index sensitivity over FOM in determining the detection limits achievable in these biosensing systems.

E Conclusions

In conclusion the rapid and straightforward highly sensitive detection of hs-CRP without the need for a wash step has been demonstrated using TSNP and Au-derived TSNP biosensors. The one-step wash-free assay method and the enhanced robust detection of the Au-edge coated TSNP demonstrate their exceptional promise for practical biosensing in the clinical setting including application in hs-CRP population screening as a tool for cardiovascular risk stratification. The stability and ensemble LSPR refractive index sensitivities of each of the Au derived TSNP sols have been examined, towards the optimisation of the nanostructures optical response for proficient detection of biosensing recognition events under physiological conditions. The stability of these nanostructures towards chloride etching promotes them above the original TSNP sols for diagnostic applications within physiological environments. Furthermore they exhibit equivalently high and enhanced ensemble LSPR refractive index sensitivities over those of the original TSNP sols. The highest ensemble refractive index sensitivity value recorded to date of 1816 nm RIU^{-1} was measured for an Au-edge-coated TSNP sol with a LSPR λ_{max} of 1197 nm. Importantly AuTSNP sensors have been demonstrated to effectively retain their high LSPR refractive index sensitivities under assay centrifugation conditions. Examination of the widely used FOM calculations highlighted its concealment of the high ensemble LSPR refractive index sensitivities of TSNP sols and Au derivative TSNP sols due to the emphasis placed on FWHM. In addition, structurally modified TSNP, namely nanomeshes and nanoboxes, revealed varying refractive index sensitivities, which did not correspond directly to the LSPR λ_{max} position. Controlled galvanic replacement processes therefore hold the potential to improve the sensitivities achievable for biosensing. The range of excellent biosensing properties of the Au-derivative TSNP sols demonstrated by our research and the methods outlined for the further enhancement of these properties, highlights the potential of the nanostructure sols for the detection of important biological molecules and clinical diagnostic applications.

Notes and references

1 K. A. Willets and R. P. Van Duyne, *Annu. Rev. Phys. Chem.*, 2007, **58**, 267–297.
2 A. J. Haes and R. P. Van Duyne, *Anal. Bioanal. Chem.*, 2004, **379**, 920–930.
3 D. E. Charles, D. Aherne, M. Gara, D. M. Ledwith, Y. K. Gun'ko, J. M. Kelly, W. J. Blau and M. E. Brennan-Fournet, *ACS Nano*, 2010, **4**, 55–64.
4 C. Xue, D. Aili and B. Liedberg, *J. Phys. Chem. C*, 2013, **117**, 23148–23154.
5 H. Wang, D. W. Brandl, F. Le, P. Nordlander and N. J. Halas, *Nano Lett.*, 2006, **6**, 827–832.
6 H. Chen, X. Kou, Z. Yang, W. Ni and J. Wang, *Langmuir*, 2008, **24**, 5233–5237.
7 E. M. Larsson, J. Alegret, M. Kall and D. S. Sutherland, *Nano Lett.*, 2007, **7**, 1256–1263.
8 M. C. Estevez, M. A. Otte, B. Sepulveda and L. M. Lechuga, *Anal. Chim. Acta*, 2014, **806**, 55–73.
9 T. W. Odom and C. L. Nehl, *ACS Nano*, 2008, **2**, 612–616.
10 J. Hurlimann, G. J. Thorbecke and G. M. Hochwald, *J. Exp. Med.*, 1966, **123**, 365–378.
11 I. Kushner, *Ann. N. Y. Acad. Sci.*, 1982, **389**, 39–48.
12 I. Kushner, M. L. Broder and D. Karp, *J. Clin. Invest.*, 1978, **61**, 235–242.
13 F. C. de Beer, C. R. Hind, K. M. Fox, R. M. Allan, A. Maseri and M. B. Pepys, *Br. Heart J.*, 1982, **47**, 239–243.
14 L. H. Kuller, R. P. Tracy, J. Shaten and E. N. Meilahn, *Am. J. Epidemiol.*, 1996, **144**, 537–547.
15 E. Haverkate, S. G. Thompson, S. D. M. Pyke, J. R. Gallimore and M. B. P. Group, *Lancet*, 1997, **349**, 462–466.
16 L. E. P. Rohde, C. H. Hennekens and P. M. Ridker, *Am. J. Cardiol.*, 1999, **84**, 1018–1022.
17 T. A. Pearson, G. A. Mensah, R. W. Alexander, J. L. Anderson, R. O. Cannon, M. Criqui, Y. Y. Fadl, S. P. Fortmann, Y. Hong, G. L. Myers, N. Rifai, N. S. C. Smith, K. Taubert, R. P. Tracy and F. Vinicor, *Circulation*, 2003, **107**, 499–511.
18 D. Aherne, D. M. Ledwith, M. Gara and J. M. Kelly, *Adv. Funct. Mater.*, 2008, **18**, 2005–2016.
19 M. M. Miller and A. A. Lazarides, *J. Phys. Chem. B*, 2005, **109**, 21556–21565.
20 D. Charles, M. Gara, D. Aherne, D. Ledwith, J. Kelly, W. Blau and M. Brennan-Fournet, *Plasmonics*, 2011, **6**, 351–362.
21 P. Mulvaney, T. Linnert and A. Henglein, *J. Phys. Chem.*, 1991, **95**, 7843–7846.

22 J. An, B. Tang, X. Zheng, J. Zhou, F. Dong, S. Xu, Y. Wang, B. Zhao and W. Xu, *J. Phys. Chem. C*, 2008, **112**, 15176–15182.

23 M. J. Banholzer, N. Harris, J. E. Millstone, G. C. Schatz and C. A. Mirkin, *J. Phys. Chem. C*, 2010, **114**, 7521–7526.

24 R. C. Doty, T. R. Tshikhudo, M. Brust and D. G. Fernig, *Chem. Mater.*, 2005, **17**, 4630–4635.

25 M. P. Brandon, D. M. Ledwith and J. M. Kelly, *J. Colloid Interface Sci.*, 2014, **415**, 77–84.

26 D. Aherne, D. E. Charles, M. E. Brennan-Fournet, J. M. Kelly and Y. K. Gun'ko, *Langmuir*, 2009, **25**, 10165–10173.

27 D. Aherne, M. Gara, J. M. Kelly and Y. K. Gun'ko, *Adv. Funct. Mater.*, 2010, **20**, 1329–1338.

28 L. J. Sherry, S. H. Chang, G. C. Schatz, R. P. Van Duyne, B. J. Wiley and Y. N. Xia, *Nano Lett.*, 2005, **5**, 2034–2038.

29 D. Thompson, M. B. Pepys and S. P. Wood, *Structure*, 1999, **7**, 169–177.

30 Y. Khalavka, J. Becker and C. Sönnichsen, *J. Am. Chem. Soc.*, 2009, **131**, 1871–1875.

31 M. A. Mahmoud, B. Snyder and M. A. El-Sayed, *J. Phys. Chem. C*, 2010, **114**, 7436–7443.

32 M. A. Mahmoud, A. J. Poncheri, R. L. Phillips and M. A. El-Sayed, *J. Am. Chem. Soc.*, 2010, **132**, 2633–2641.

33 J. B. Lassiter, H. Sobhani, J. A. Fan, J. Kundu, F. Capasso, P. Nordlander and N. J. Halas, *Nano Lett.*, 2010, **10**, 3184–3189.

34 C. L. Nehl, H. W. Liao and J. H. Hafner, *Nano Lett.*, 2006, **6**, 683–688.

35 J. Henzie, M. H. Lee and T. W. Odom, *Nat. Nanotechnol.*, 2007, **2**, 549–554.